Mon. Not. R. Astron. Soc. 293, 325–336 (1998)

HST imaging of the globular clusters in the Fornax cluster: NGC 1399 and NGC 1404

Duncan A. Forbes,[1★] Carl J. Grillmair,[2★] Gerard M. Williger,[3,4★] R. A. W. Elson[5★] and Jean P. Brodie[6★]

[1]*School of Physics and Astronomy, University of Birmingham, Edgbaston, Birmingham B15 2TT*
[2]*Jet Propulsion Laboratory, 4800 Oak Grove Drive, Pasadena, CA 91109, USA*
[3]*MPIA, Königstuhl 17, D-69117 Heidelberg, Germany*
[4]*NOAO, Code 681, Goddard Space Flight Center, Greenbelt, MD 20771, USA*
[5]*Institute of Astronomy, Madingley Road, Cambridge CB3 0HA*
[6]*Lick Observatory, University of California, Santa Cruz, CA 95064, USA*

Accepted 1997 September 22. Received 1997 September 10; in original form 1997 June 20

ABSTRACT

The Fornax cluster galaxies NGC 1399 and NGC 1404 are ideal for studying the effects of a cluster environment on globular cluster systems. Here we present new optical imaging of these two galaxies from both the *Hubble Space Telescope*'s Wide Field and Planetary Camera 2 and the Cerro Tololo Inter-American Observatory 1.5-m telescope. The combination of both data sets provides a unique insight on the spatial and colour distribution of globular clusters. From $B-I$ colours, we find that both galaxies have a broad globular cluster metallicity distribution that is inconsistent with a single population. Two Gaussians provide a reasonable representation of the metallicity distribution in each galaxy. The metal-rich subpopulation is more centrally concentrated than the metal-poor one. We show that the radial metallicity gradient can be explained by the changing relative mix of the two globular cluster subpopulations. We derive globular cluster surface density profiles, and find that they are flatter (i.e., more extended) than the underlying starlight. The total number of globular clusters and specific frequency are calculated to be $N=5700\pm500$, $S_N=11.5\pm1.0$ for NGC 1399, and $N=725\pm145$, $S_N=2.0\pm0.5$ for NGC 1404. Our results are compared with the expectations of globular cluster formation scenarios.

Key words: galaxies: clusters: individual: Fornax – galaxies: elliptical and lenticular, cD – galaxies: individual: NGC 1399 – galaxies: individual: NGC 1404 – galaxies: interactions – galaxies: star clusters.

1 INTRODUCTION

Globular cluster (GC) systems are in some respects (e.g., luminosity function) more similar to one another than are their host galaxies. This suggests an underlying uniformity in the physical conditions under which GC systems and galaxies formed. On the other hand, properties such as the total number of clusters per unit galaxy luminosity show significant variations, and fundamental questions concerning the origins of these variations remain unanswered. In particular, the roles of tidal encounters, mergers, cooling flows, and initial conditions in the formation of GC systems have yet to be understood.

Two galaxies of particular interest in this regard are NGC 1399 at the centre of the Fornax cluster, and a nearby cluster member, NGC 1404. By studying the GC systems of these two galaxies we hope to understand better the environmental influences on the formation of GCs and their host galaxies. Various estimates of the distance modulus to the Fornax cluster have been made in recent years. Here we

★E-mail: forbes@star.sr.bham.ac.uk (DAF);
carl@grandpa.jpl.nasa.gov (CJG);
williger@tejut.gsfc.nasa.gov (GMW);
elson@star.ast.cam.ac.uk (RAWE);
brodie@ucolick.org (JPB)

adopt a typical value of $m-M=31.2$, which places the cluster 0.2 mag more distant than Virgo (Jacoby et al. 1992). With this distance modulus and no Galactic extinction correction, the optical luminosity of NGC 1399 is $M_V=-21.74$ (Faber et al. 1989). This cD galaxy is surrounded by hot X-ray-emitting gas, which extends out to at least 38 arcmin or 190kpc (Mason & Rosen 1985; Ikebe et al. 1996). The mass-to-light ratio increases with galactocentric distance, reaching a value of $M/L \sim 70\ M_\odot/L_\odot$ at ~ 5 arcmin (Grillmair et al. 1994a). Well within the X-ray envelope, even allowing for projection effects, at about 10 arcmin (50 kpc) to the south-east of NGC 1399 lies NGC 1404. It is classified as an E1 galaxy and has an optical luminosity of $M_V=-21.37$ (Faber et al. 1989).

The GC systems of NGC 1399 and 1404 have been studied using ground-based imaging by a number of workers (NGC 1399: Hanes & Harris 1986; Giesler & Forte 1990; Bridges, Hanes & Harris 1991; Wagner, Richtler & Hopp 1991; Ostrov, Geisler & Forte 1993; Kissler-Patig et al. 1997, and NGC 1404: Hanes & Harris 1986; Richtler et al. 1992). For NGC 1399, Kissler-Patig et al. (1997) give the total number of GCs as $N_{GC}=5940\pm570$. This gives a high specific frequency $S_N=11\pm4$. A kinematic study of the GCs around NGC 1399 showed that the outer GCs appear to be dynamically related more to the cluster of galaxies than they are to NGC 1399 itself (Grillmair et al. 1994a). This suggests that accretion of intracluster GCs (West et al. 1995), tidal stripping (Forte, Martinez & Muzzio 1982; Forbes, Brodie & Grillmair 1997b) or mergers (Ashman & Zepf 1992) may help to explain the high specific frequency of NGC 1399. For NGC 1404 the number of GCs is less certain. Hanes & Harris (1986), from a photographic study, estimated $N_{GC}=190\pm80$, while more recently Richtler et al. (1992) found $N_{GC}=880\pm120$. The resulting S_N values range from 0.5 ± 0.3 to 2.5 ± 0.3 respectively. The latter value is close to the average for ellipticals in the Fornax cluster.

Here we present imaging data from *HST*'s Wide Field and Planetary Camera 2 (WFPC2) and the Cerro Tololo Inter-American Observatory's (CTIO) 1.5-m telescope of NGC 1399 and NGC 1404. The WFPC2 data provide accurate magnitudes and colours, with virtually no contamination from foreground stars or background galaxies. These data are complemented by wide field-of-view CCD imaging from CTIO. In this paper we will focus on the colour (metallicity) and spatial distribution of GCs. The GC luminosity functions in these two galaxies and others in the Fornax cluster are addressed by Grillmair et al. (1997), and a detailed study of NGC 1379, using WFPC2 and CTIO data, is given by Elson et al. (1997).

2 OBSERVATIONS AND DATA REDUCTION

2.1 *HST* imaging

Details of our *HST* imaging programme are given by Grillmair et al. (1997). Here we use four pointings from that programme, namely a central pointing on each of NGC 1399 and NGC 1404, an outer pointing for NGC 1399, and a background field. The outer pointing (F0338) is situated in the cD envelope of NGC 1399, on the opposite side of the galaxy from NGC 1404. The background field (F0336) is situated approximately $1\overset{\circ}{.}4$ south of NGC 1399 in a blank region of sky and serves to measure the surface density of background sources.

Exposure times totalled 1800 s in F814W and 5200 s in F450W for NGC 1399 and 1860 and 5000 s for NGC 1404 using the WFPC2 camera. Three images were taken at one pointing; the other two were offset by 0.4 arcsec, which corresponds roughly to integer pixel shifts in both the PC and WFC chips. The images were then aligned and median-combined using VISTA software, which effectively removed both cosmic rays and hot pixels. The resulting images were found to be statistically superior to those reduced using standard STSDAS tasks, and this enabled us to push our completeness limit to about $B=26.5$ without incurring large numbers of spurious detections.

Compact sources in each pointing have been detected and measured using DAOPHOT II/ALLSTAR software, as described in Grillmair et al. (1997). For the PC chips the galaxy was subtracted off first. Magnitudes have been converted into standard Johnson–Cousins B and I. No Galactic extinction correction has been applied. A colour–magnitude diagram for all of the detected sources in each of the four pointings is shown in Fig. 1. Completeness tests indicate that the 50 per cent incompleteness occurs at $B\sim26.5$ for all four pointings, with small variations between each pointing. (Note for the PC chips it is about 0.5 mag brighter.) In order to avoid any colour bias in our results, we have excluded all sources fainter than this limit. We have also excluded sources brighter than $B=21$, as these objects would be more luminous than Galactic GCs, and so are probably foreground stars. We also applied a colour cut to the data, so that only sources with $1.2<B-I<2.5$ are included. This cut is roughly equivalent to $-2.5<[\mathrm{Fe/H}]<+1.0$, assuming the Galactic colour–metallicity relation of Couture, Harris & Allwright (1990), and covers the range of expected GC metallicities. For NGC 1399, 95 per cent of all sources lie within this colour selection, and for NGC 1404 it is 90 per cent. This magnitude and colour selection are indicated in Fig. 1 by dashed lines. With these selection cuts applied, our final sample consists of 572 objects in NGC 1399 central, 59 in NGC 1399 outer, and 208 in NGC 1404. The background field has only 14 objects. This background field allows us to estimate fairly accurately the proportion of *bona fide* GCs in the three galaxy pointings, i.e., ≥98 per cent in NGC 1399 central, ≥76 per cent in NGC 1399 outer, and ≥93 per cent in NGC 1404.

2.2 Ground-based imaging

Broad-band B and I images of NGC 1399 and NGC 1404 were taken with the CTIO 1.5-m telescope. We used a Tek 2048×2048 array with a pixel scale of 0.44 arcsec pixel^{-1}, yielding a field-of-view 15 arcmin on a side. The galaxies were observed in 1995 December with typical seeing conditions of ~1.5 arcsec. Data reduction was carried out in the standard way (i.e., bias and dark-current subtraction, flat-fielding and sky subtraction). The total exposure times were 9600 s in B and 3660 s in I for NGC 1399, and 9100 s in B and 3060 s in I for NGC 1404. After combining, the images were calibrated using aperture photometry from the catalogues of Longo & de Vaucouleurs (1983) and de Vaucouleurs & Longo (1988). This procedure gave an rms accuracy

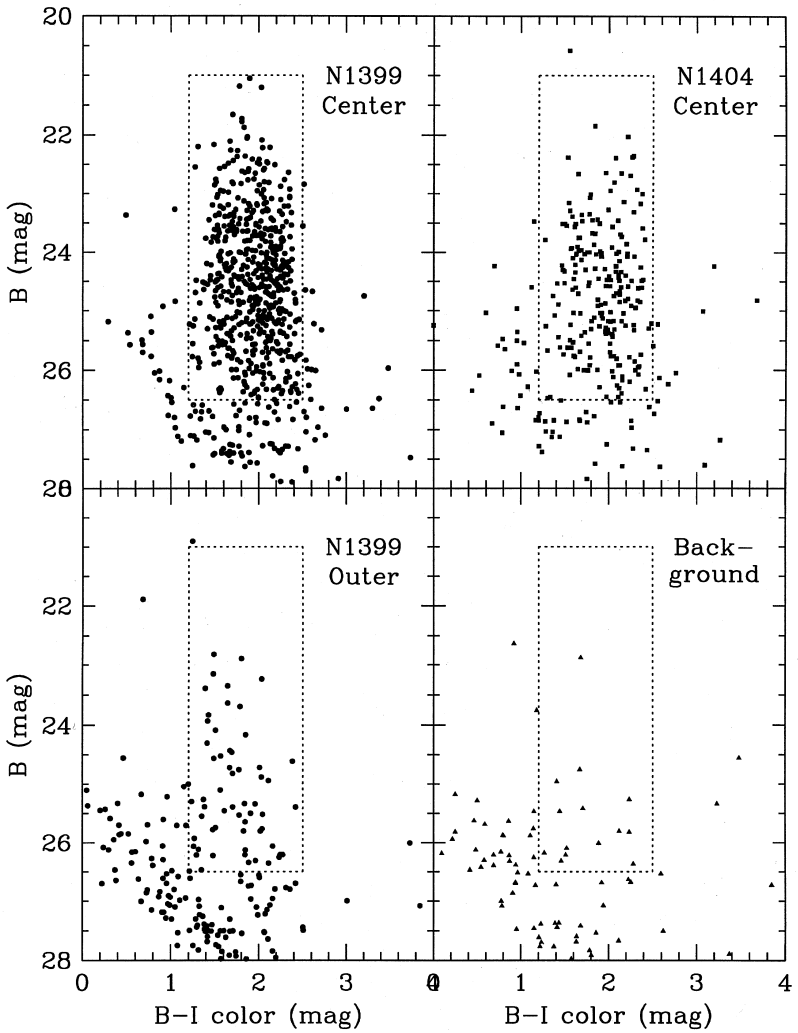

Figure 1. Colour–magnitude diagrams for the compact objects in four *HST* pointings: central NGC 1399 (circles), central NGC 1404 (squares), outer NGC 1399 (circles) and a background field (triangles). The dashed box indicates the colour and magnitude selection criteria (see text for details).

of ± 0.08 mag for NGC 1399, and ± 0.05 mag for NGC 1404. No Galactic extinction correction was applied.

Globular clusters were detected automatically using DAOPHOT. The detection threshold was set at a conservative 5σ per pixel, i.e. five times the background noise. Selection cuts in the DAOPHOT 'sharpness' and 'roundness' parameters were made to help remove cosmic rays and extended objects from the candidate lists. (These parameters help to remove spiky objects and very non-round objects.) For each detected object we measured a 3-pixel-radius aperture magnitude and applied an aperture correction based on a curve-of-growth type analysis for a dozen isolated GCs. The rms from the aperture correction is ~ 0.05 mag. Colour–magnitude diagrams for all of the detected sources for the two galaxies are shown in Fig. 2. For the CTIO data we decided to adopt the same colour selection criteria as the *HST* data, and the same bright magnitude cut-off. For the faint magnitude cut-off, we use the 50 per cent incompleteness value. Based on an examination of the luminosity function, we estimate that for NGC 1399 the 50 per cent value is $B \sim 24.3$, and for NGC 1404 it is $B \sim 24.4$. Thus our CTIO selection criteria are $1.2 < B-I < 2.4$ and $21 < B < 24.2/24.3$, as is indicated in Fig. 2 by dashed lines. Even with our selection criteria we expect some contamination from foreground stars and background galaxies in our samples of 1752 objects in NGC 1399 and 858 objects in NGC 1404. This issue will be discussed below. We note that although the CTIO data only sample the brighter GCs, we do not expect this to bias the metallicity distribution. For GCs in the Milky Way and M31 (Huchra, Brodie & Kent 1991) and in NGC 5846 (Forbes, Brodie & Huchra 1996a) there appears to be no luminosity–metallicity dependence.

3 RESULTS AND DISCUSSION

3.1 Spatial distribution

Given the magnitude depth and the availability of a background field, our *HST* data are ideal for examining the surface density distribution of GCs. We first calculate the GC density in five annuli around NGC 1399. We make use of the fact that out to 100-arcsec radius the WFPC2 gives

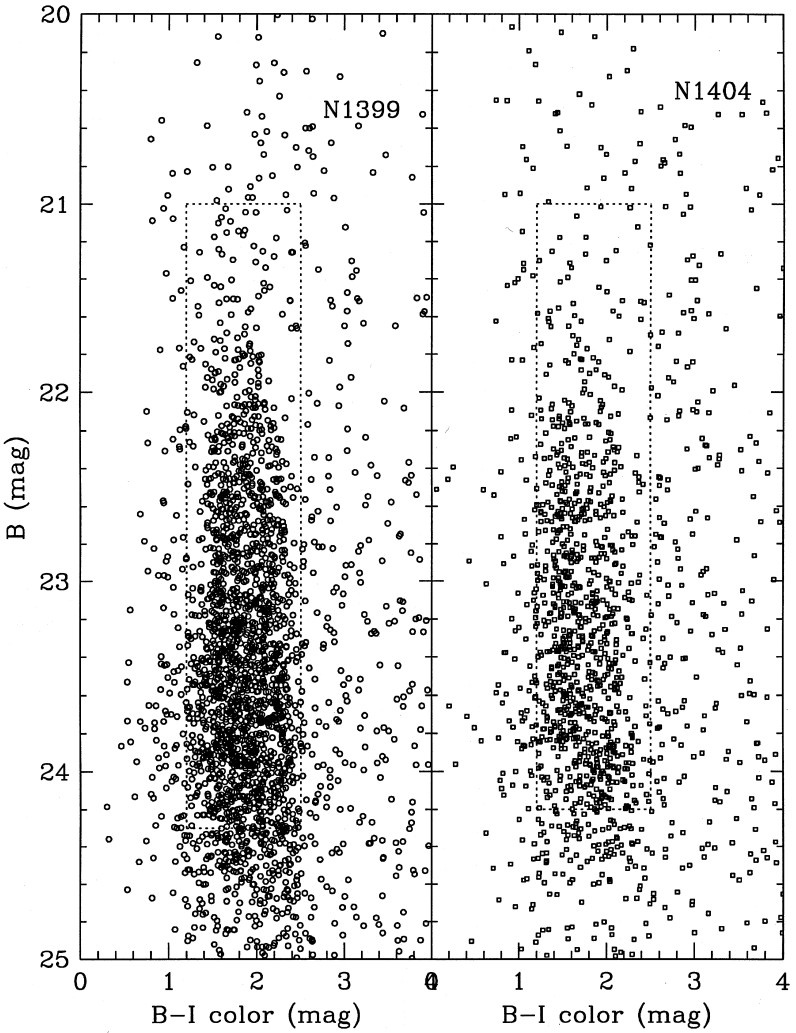

Figure 2. Colour–magnitude diagrams for the compact objects in two CTIO pointings centred on NGC 1399 (circles) and NGC 1404 (squares). The dashed box indicates the colour and magnitude selection criteria (see text for details).

almost complete 180° coverage for one hemisphere of the galaxy (see Forbes, Franx & Illingworth 1995 for details). For the NGC 1399 outer and background fields we simply add up the total number of GCs, i.e., 59 and 14 respectively. We have also made a small correction ($\sim$15 per cent) for the expected number of undetected GCs at the faint end of the luminosity function as determined by Grillmair et al. (1997). Next, we divide the number of GCs by the appropriate spatial coverage to give a surface density. Finally, we subtract off the background density of 2.9 objects per square arcmin, giving the background-corrected surface density of GCs. This is shown in Fig. 3.

Excluding the innermost two data points for NGC 1399, we have fitted the data with a function of the form

$$\rho = \rho_0 r^{\alpha}.$$

This fit is shown by a solid line for which $\rho_0 = 126$ arcmin^{-2} and $\alpha = -1.2 \pm 0.2$. It is clear from the NGC 1399 outer pointing that there are GCs at a projected radius of 8.2 arcmin from NGC 1399. Extrapolation of the profile to 9.7 arcmin (the projected distance of NGC 1404) suggests that there is about one GC per square arcmin associated with NGC 1399. This corresponds to half a dozen GCs in the WFPC2 field-of-view centred on NGC 1404. The procedure for estimating the surface density profile of NGC 1404 is similar to that of NGC 1399, except that we subtract both the background density and the expected density of GCs in each annulus due to NGC 1399. Again the *HST* data are fitted using a power-law profile (excluding the innermost data point) with $\rho_o = 36$ arcmin^{-2} and $\alpha = -1.3 \pm 0.2$.

For both galaxies the GC surface density rises towards the galaxy centre but flattens off (in log space) in the very inner regions, giving a definable 'core' to the GC system where the profile changes slope. This does not appear to be a selection effect, and it has been observed in other large galaxies (e.g. Grillmair, Prichet & van den Bergh 1986; Grillmair et al. 1994b). Forbes et al. (1996b) found that the 'core radius' of the GC system is loosely correlated with the galaxy luminosity. We estimate that the GC systems of NGC 1399 and NGC 1404 have core radii of 40 arcsec (3.4 kpc) and 30 arcsec (2.5 kpc) respectively. These values are within the scatter of the relation found by Forbes et al. (1996b), and are similar to the galaxy effective radii. We have measured a GC surface density slope of -1.2 ± 0.2 for NGC 1399.

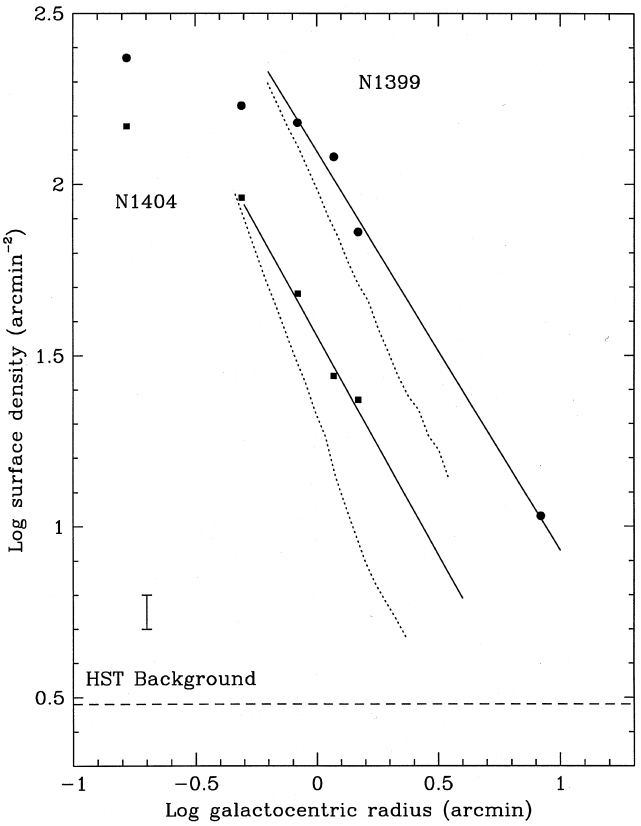

Figure 3. Surface density profiles for the globular cluster systems in NGC 1399 (circles) and NGC 1404 (squares) from *HST* data. The surface densities have had a correction for background contamination and for the missing faintest globular clusters. The globular cluster systems of both galaxies reveal a 'core region'. Power-law fits to the data beyond the core region are shown by solid lines. The surface density of compact background objects in *HST* images is shown by a long-dashed line. A typical error bar is shown on the left. The underlying galaxy starlight profile, arbitrarily normalized in the vertical direction, is shown by a short-dashed line. For both galaxies the starlight is more concentrated than the globular cluster system.

There have been three previous CCD studies which measured the GC slope. Wagner et al. (1991) found that interior to $\sim$120 arcsec the GC slope was -1.4 ± 0.11, and this steepened to -1.54 ± 0.15 for larger radii. Kissler-Patig et al. (1997) derived -1.55 ± 0.25 and -1.75 ± 0.3 from two pointings for radii beyond $\sim$50 arcsec. Bridges et al. (1991) measured -1.4 ± 0.2 from their *B*-band data, and -1.5 ± 0.2 from their *V*-band data. Our value is somewhat flatter than those measured by others. One possible reason for this is that our outer pointing is located in the cD envelope of NGC 1399 where the GC surface density 'flattens out' (e.g. Kissler-Patig et al. 1997). If we exclude the outer point, our fitted slope steepens to -1.25. Another possibility is that, even though we have not included the inner two data points in the fit, we are still fitting into the core-flattened region. The stellar profile (log intensity) for NGC 1399 is also shown in Fig. 3. We measure a slope of -1.6 ± 0.1 for the galaxy light. This compares with the measurements of -1.67 ± 0.12 (Wagner et al. 1991) and -1.75 ± 0.1 (Kissler-Patig et al. 1997). There has been some debate as to whether the GC profile is flatter than the galaxy profile in NGC 1399. In particular, Bridges et al. (1991) claimed that the GC system has the same slope as the galaxy, whereas both Wagner et al. (1991) and Kissler-Patig et al. (1997) said that it is somewhat flatter. Excluding our data, the weighted mean value from previous studies is -1.47 ± 0.09 for the GC slope, and -1.72 ± 0.06 for the galaxy slope. This indicates that the GC profile is 0.25 ± 0.11 flatter than the galaxy starlight. Our data suggest that the difference is even greater, i.e., 0.4 ± 0.22. Thus we conclude that the GC surface density profile is flatter than the galaxy starlight by about 0.3 in the log at about the 2σ significance level. For NGC 1404, we measure a GC slope of -1.3 ± 0.2 and a galaxy starlight slope of -1.9 ± 0.1. Thus the GC systems in both galaxies have a flatter, more extended distribution than the underlying starlight.

Using the surface density profile, we can estimate the total number of GCs and the specific frequency (S_N; Harris & van den Bergh 1981) for NGC 1399 and NGC 1404. For NGC 1399 the GCs clearly extend beyond 8 arcmin in our data. We have decided to use 10 arcmin as the limiting radius, which is the same limit used by Hanes & Harris (1986) in their photographic study. Integrating the power-law profile between $\log r=-0.2$ (38 arcsec) and 1 (10 arcmin), and adding the number of GCs interior to 38 arcsec gives a total of 5700 GCs. The uncertainty in deriving the total number of GCs is dominated by the choice of limiting radius. We have used ±1 arcmin about the limiting radius as our error estimate. Thus limiting radii of 9 and 11 arcmin give $N=5700\pm500$. This is in good agreement with the determination of Kissler-Patig et al. (1997) of $N=5940\pm570$. For an absolute magnitude of $M_V=-21.74$, the specific frequency $S_N=11.5\pm1.0$.

For NGC 1404 the limiting radius is difficult to estimate. Richtler et al. (1992) determined a background level at $\sim$200 arcsec. We find that in the direction of NGC 1399, the density of GCs is clearly dominated by NGC 1399 beyond about 250 arcsec. We have chosen to integrate out to 240 arcsec (4 arcmin) with a reasonable range of 3–5 arcmin. Thus, integrating the profile from $\log r=-0.3$ (30 arcsec) to 0.6 (4 arcmin) and adding the number of inner GCs gives $N=725\pm145$ GCs associated with NGC 1404. This lies between the Hanes & Harris (1986) value (190 ± 80) and the Richtler et al. (1992) value (880 ± 120). Compared to these ground-based studies, our *HST* data have the advantages of accurate background subtraction (star, galaxies and NGC 1399 GCs) and nearly complete magnitude coverage. For an absolute magnitude of $M_V=-21.37$, our results indicate a relatively low specific frequency for NGC 1404 of $S_N=2.0\pm0.5$. Again using the *HST* data, we calculate the 'local' S_N values (i.e. using the number of GCs and the integrated magnitude at the de Vaucouleurs effective radius) to be $\sim$1.5 for NGC 1399, and $\sim$0.5 for NGC 1404.

In Figs 4 and 5 we show the azimuthal distribution of GCs, as determined from the *HST* data, over the range for which we have uniform radial and azimuthal coverage. For NGC 1399 (Fig. 4) slight enhancements in the GC counts can be seen close to the major axes of the galaxy (position angles PA $\sim100°$ and $-80°$). There is also a slight deficit around the minor axis PA $\sim10°$. Thus the GC system is broadly aligned with the stellar isophotes. The direction

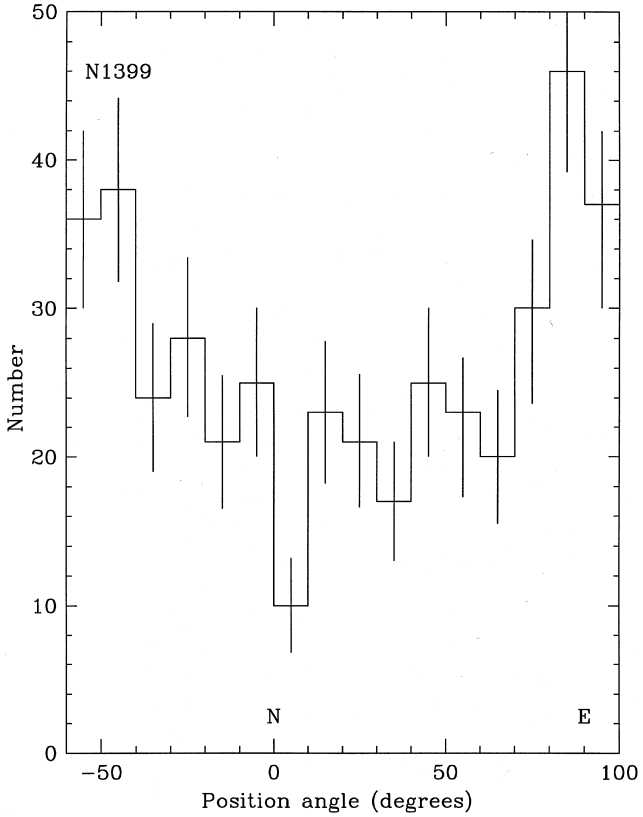

Figure 4. Histogram of globular cluster position angles within 100-arcsec radius of NGC 1399, from *HST* data of the galaxy. The major axes of the galaxy are at PA $\sim 100°$ and $-80°$. Globular clusters appear to be concentrated close to the major axis of the galaxy and show a deficit along the minor axis.

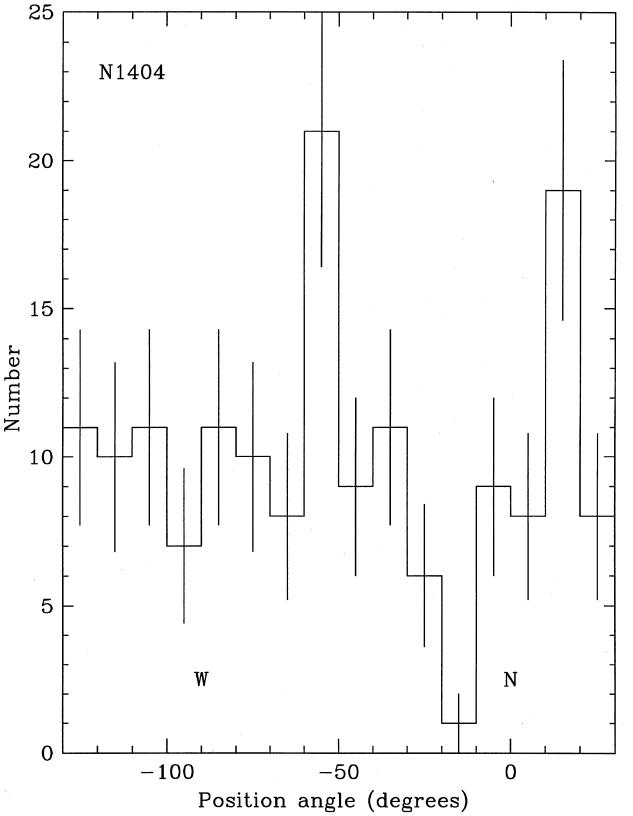

Figure 5. Histogram of globular cluster position angle within 100 arcsec of NGC 1404, from *HST* data. The major axis of the galaxy is at PA $\sim -20°$. Globular clusters appear to show a slight deficit near the major axis of the galaxy.

towards NGC 1404 (PA $\sim 150°$) is not covered by our *HST* image. For NGC 1404, shown in Fig. 5, there is a slight deficit in GC counts along the major axis of the galaxy at PA $\sim -20°$. There are also two enhancements at PA $\sim -50°$ and 10° which do not correspond to either the major or minor axis of the galaxy.

3.2 Colour and metallicity distributions

The GC colour distributions, after colour and magnitude selection, for the four *HST* pointings are shown in Fig. 6. Both NGC 1399 and NGC 1404 are dominated by red ($B-I \sim 2.1$) GCs, but with a significant tail to the blue (i.e. $B-I \sim 1.6$). The GCs in the outer pointing of NGC 1399 are bluer on average than those in the central pointing. The median colours are $B-I = 1.97$ for NGC 1399 in the central pointing, 1.70 for the outer NGC 1399 pointing, and 1.96 for NGC 1404.

The CTIO data, after colour and magnitude selection, are shown in Fig. 7. We do not have a background field for the CTIO data. Although we have attempted to remove galaxies using the DAOPHOT sharpness and roundness parameters, our seeing conditions of ~ 1.5 arcsec imply that some galaxies will be included in our candidate list. The issue of background galaxy contamination in GC colour/metallicity distributions is discussed in some detail by Elson et al. (1997). Background galaxies in our magnitude range peak at $B-I \sim 1.0$ and become bluer at fainter magnitudes. The galaxy counts are falling fast at our blue cut-off of $B-I = 1.2$. Given the richness of the NGC 1399 GC system, background galaxies are likely to be a small affect. However, it may be more of a concern for NGC 1404. We can estimate the effects of background contamination using the CFRS sample (Lilly et al. 1995) within the appropriate B magnitude range and scaled in area to match that of the CTIO data. The background-corrected distributions are shown by a dashed line in Fig. 7. As we have already removed some galaxies in our initial detection process, the true distribution may lie somewhere between the two histograms. In either case (uncorrected or corrected) the distributions reveal a somewhat different situation to the *HST* data, with the GC systems in both galaxies peaking in the blue ($B-I \sim 1.6$) with a significant red tail (around $B-I \sim 2.1$). The median colours are $B-I = 1.84$ for NGC 1399, and 1.71 for NGC 1404. Thus the CTIO colours are on average systematically ~ 0.1 mag bluer than the *HST* data. This result is not formally significant, as the error is also on the order of 0.1 mag, but differences between the shape of the two distributions are clearly seen. As the *HST* data cover only the central regions of each galaxy, this suggests a radial colour gradient from red-dominated objects at small galactocentric radii to blue ones further out. In principle, such a gradient could be caused by blue background galaxies in the CTIO

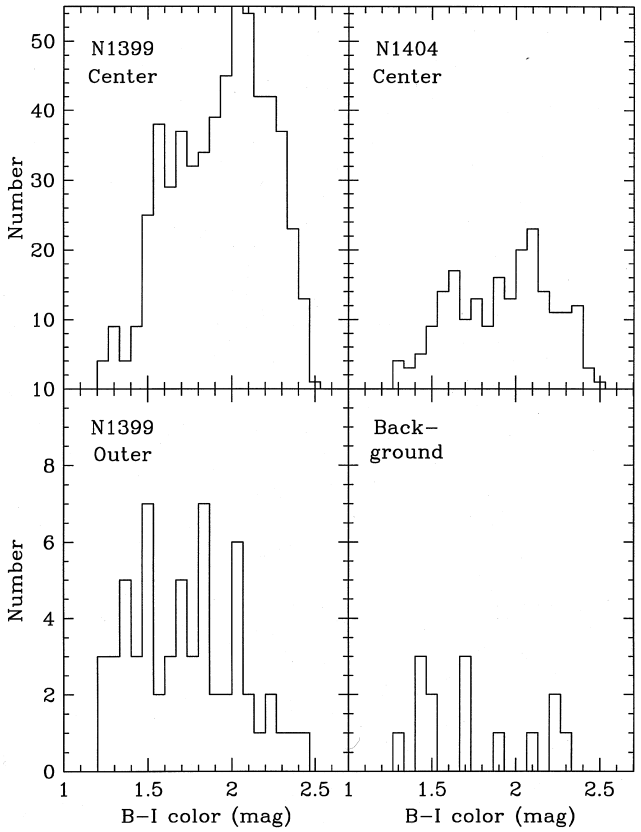

Figure 6. Histograms of globular cluster $B-I$ colours for the four *HST* pointings. In the central pointings, both galaxies are dominated by red globular clusters with an extended blue tail.

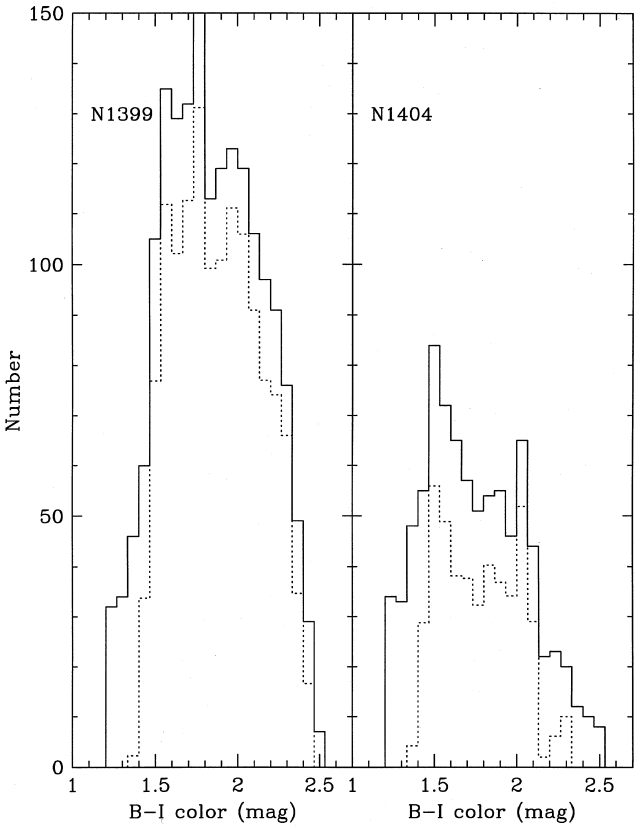

Figure 7. Histograms of globular cluster $B-I$ colours for the two CTIO pointings. The dashed line shows the distribution after correction for background contamination. In these wide-area pointings, both galaxies are dominated by blue globular clusters with an extended red tail.

data. However, we give further evidence below that this is not the case.

In Fig. 8 we show the GC colour distributions for NGC 1399 and NGC 1404 from the *HST* data. Here the data for NGC 1399 includes both the central and outer pointing. The background-corrected histograms are shown by dashed lines. Some galaxies, such as M87 (Whitmore et al. 1995; Elson & Santiago 1996), reveal a clear bimodal GC colour distribution. In other cases (i.e., NGC 1374, 1379, 1387 and 1427) the distribution is essentially consistent with a single unimodal colour for the GC system (Kissler-Patig et al. 1997; Kissler-Patig, Forbes & Minniti 1997; in preparation). The situation for NGC 1399 and 1404 is not as clear. Nevertheless, there is some evidence for multiple GC populations. First, both galaxies have distributions that are significantly broader than that expected from the photometric errors (typically $\sigma \sim 0.15$), i.e., there is a real spread in GC colours. Secondly, we have tested the unbinned colour data using the KMM statistical test (Ashman, Bird & Zepf 1994). This test rejects a single Gaussian fit to the NGC 1399 and NGC 1404 data with a confidence of over 99 per cent. If we represent the data by two Gaussians, then the KMM test determines means of $B-I=1.7$ and 2.1 for NGC 1399, and $B-I=1.6$ and 2.1 for NGC 1404. Thirdly, as an exercise, we generated a colour histogram that is the sum of two Gaussians. These Gaussians have mean colours of $B-I=1.6$ and 2.1, with dispersions similar to the photometric error, and with total numbers in the ratio of 1:4. They are shown in the lower left panel of Fig. 8. In the lower right panel, we show the same two Gaussians, but with alternating Poisson noise included. To the eye, the two noisy Gaussians are qualitatively similar to the *HST* data, suggesting that they could consist of two Gaussian-like populations. Fourthly, the two peaks indicated in the *HST* data are also present in the CTIO data (Fig. 7). *We conclude that both galaxies do not have a single, uniform GC population, but rather show evidence for a multimodal GC colour distribution.*

Two other large data sets exist for GCs in NGC 1399. They are the CTIO 4-m observations by Ostrov et al. (1993) using Washington photometry, and the Las Campanas 2.5-m observations by Kissler-Patig et al. (1997) in V and I. In order to compare all of the different data sets, we have converted each into metallicity. Broad-band colours can be transformed into metallicity using the Galactic relation of Couture et al. (1990), given the usual caveat that age effects and abundance anomalies may be present. The Washington photometry of Ostrov et al. is transformed using the relation derived by Geisler & Forte (1990). Washington photometry is the most sensitive to metallicity (rms ~ 0.1), then $B-I$ colours (rms ~ 0.15) with $V-I$ colours being the least sensitive (rms ~ 0.25). In Fig. 9 we show the GC metallicity distributions from our *HST* and CTIO data sets, along with those of Ostrov et al. and Kissler-Patig et al. None of the

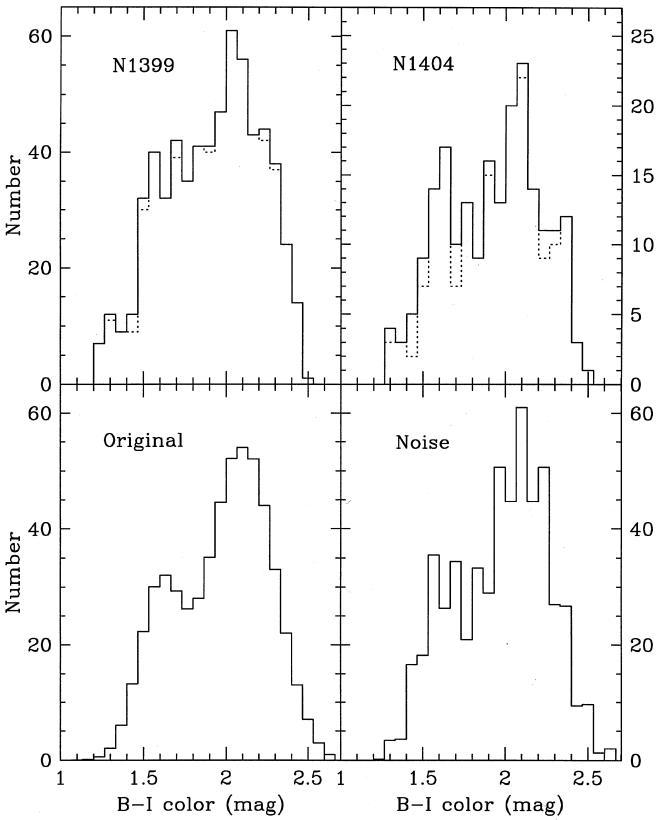

Figure 8. Histograms of the globular cluster $B-I$ colours in NGC 1399 and 1404 from *HST* data (upper panels). For NGC 1399 the central and outer pointings have been co-added. The dashed line shows the distribution after correction for background contamination. The lower left panel shows the sum of two Gaussians with peaks at $B-I=1.6$ and 2.1. The lower right panel shows the same two Gaussians with Poisson noise included. The metallicity distribution of both galaxies can be plausibly represented by two Gaussians.

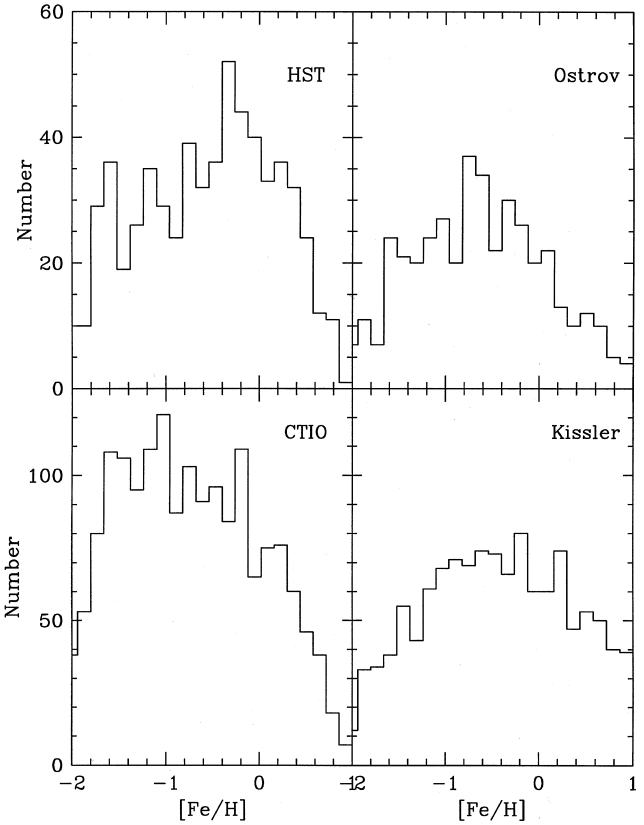

Figure 9. The metallicity distribution for globular clusters in NGC 1399 from four different samples. Data from this paper are shown in the left-hand side panels. The upper right panel shows the data of Ostrov et al. (1993), and the lower right panel shows the data of Kissler-Patig et al. (1997). None of the samples shown here has been background corrected (although for the *HST* sample this is negligible). The Ostrov et al. data have the highest metallicity sensitivity. The *HST* distribution is inconsistent with a single Gaussian and is better described as multimodal. Common peaks (particularly at [Fe/H] ~ -0.2) can be seen in each data set.

data sets has been background-corrected in this figure (although for the *HST* sample the correction is negligible). In general, the samples reveal a broad distribution with several minor enhancements, many of which appear common to several data sets. From their data, Ostrov et al. claimed that NGC 1399 has a trimodal GC metallicity distribution, with peaks at [Fe/H] ~ -1.5, -0.8 and -0.2. The metal-rich peak corresponds to that seen clearly in our *HST* data. The two metal-poor peaks may be real or simply a single population with [Fe/H] ~ -1.0. The mean $B-I$ colours found by the KMM test on the *HST* data correspond to [Fe/H] ~ -1.1 and -0.1. The GC metallicity distribution for NGC 1404 from our *HST* data is shown in Fig. 10. As indicated by the KMM test, a bimodal distribution is a better representation of the data than a single Gaussian. The two GC populations have means of [Fe/H] ~ -1.5 and -0.1.

We now return to the CTIO data and the issue of background contamination. Earlier we argued that contamination, although present, did not change the basic appearance of the colour distributions. Further evidence that the two peaks in the CTIO data are dominated by *bona fide* GCs comes from examining the spatial distribution of the two subpopulations. First, we define the metal-rich and metal-poor GC subpopulations in each galaxy as being ± 0.3 dex about the mean metallicity of each subpopulation. We then calculate the raw surface density (i.e. not corrected for background contamination or for the missing faint end of the luminosity function) for the two subpopulations. These surface density profiles are shown in Fig. 11. A background correction would tend to lower the metal-poor profile, particularly at galactocentric radii beyond 4 arcmin in NGC 1404 (which is excluded from the figure). Although there is considerable scatter, the surface density of each subpopulation declines with distance from its parent galaxy. This indicates that each subpopulation is associated with the galaxy and is therefore dominated by GCs. Secondly, the fact that the *HST* colours (metallicities) agree with those in the inner annuli of the CTIO data (see Figs 12 and 13) indicates that the subpopulations are dominated by GCs.

Next, we investigate the radial variation of GC metallicity. We have seen that for both NGC 1399 and NGC 1404, the metal-rich (red) subpopulation dominates in the *HST* data, while in the CTIO data the metal-poor (blue) subpopulation is dominant. As the *HST* data probe

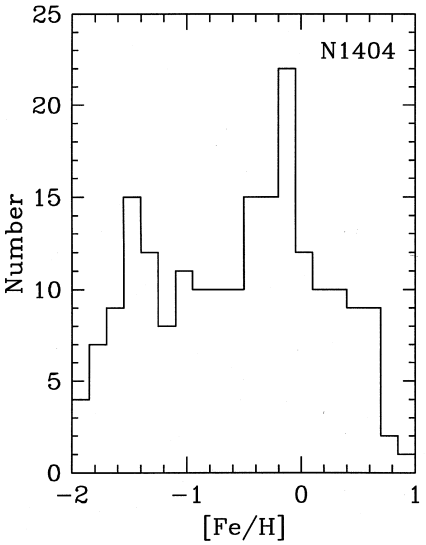

Figure 10. The metallicity distribution for globular clusters in NGC 1404 from *HST* data. A KMM test indicates that the distribution is inconsistent with a single Gaussian, and that a bimodal distribution with mean metallicites of [Fe/H] ~ -1.5 and -0.1 provides a better fit.

the inner $\sim$100-arcsec region and the CTIO data cover the regions beyond $\sim$30 arcsec, this would suggest that the metal-rich GCs are more centrally concentrated than the metal-poor ones. A similar situation is inferred for NGC 4472 (Geisler, Lee & Kim 1996) and NGC 5846 (Forbes, Brodie & Hurhra 1997a). An unweighted fit to the *HST* data indeed indicates a metallicity gradient in both galaxies. For NGC 1399 we find [Fe/H] $= -0.31 \pm 0.13$ log R (arcsec) $- 0.046 \pm 0.22$. This slope is similar to that found by Ostrov et al. (1993), i.e., -0.34 ± 0.18. The fit for NGC 1404 gives [Fe/H] $= -0.36 \pm 0.13$ log R (arcsec) $- 0.034 \pm 0.22$. In both cases the *HST* fits are consistent with the CTIO data. In NGC 4472, Geisler et al. (1996) found that the radial GC metallicity gradient was actually due to the changing relative mix of the two GC subpopulations. Assuming that NGC 1399 and NGC 1404 can be represented by metal-rich and metal-poor GC subpopulations, we investigate the radial gradients further.

In Figs 12 and 13 we show the metallicity in various radial bins for the different GC subpopulations and the mean metallicity for the combined population. The range in metallicity included in each data point is ± 0.3 dex. For NGC 1399 (Fig. 12) the metal-poor and metal-rich GC subpopulations show no obvious radial metallicity gradient. However, the mean values for the whole GC system *do* show a global radial gradient. Though not quite as convincing, the same trend appears to be true for NGC 1404 (Fig. 13). For both galaxies, we conclude that the radial metallicity gradient for the overall GC system is consistent with the changing relative proportions of the GC subpopulations; the metal-rich GCs are centrally concentrated, while the metal-poor ones are preferentially located in the outer regions. The lack of a real abundance gradient places constraints on the role of gas dissipation in the formation of GCs. In NGC 4472, the metallicity of the galaxy field stars was found to be of the same as, or of slightly higher than, the metal-rich GCs (Geisler et al. 1996). For NGC 1399, Brodie & Huchra (1991) quote a spectroscopic metallicity of

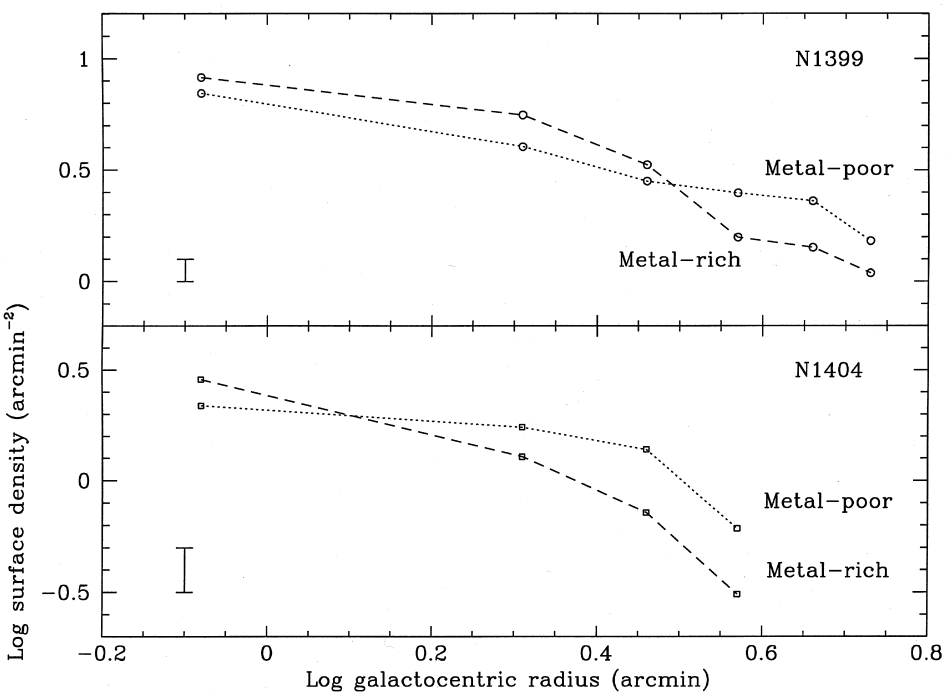

Figure 11. Surface density profiles for the metal-rich and metal-poor globular cluster subpopulations in NGC 1399 (circles) and NGC 1404 (squares) from CTIO data. No correction has been applied for background contamination or missing globular clusters at the faint end of the luminosity function. Typical data error bars are shown on the left. In both galaxies the two subpopulations decline with galactocentric radius, indicating that they are dominated by globular clusters. The metal-rich subpopulation is more centrally concentrated.

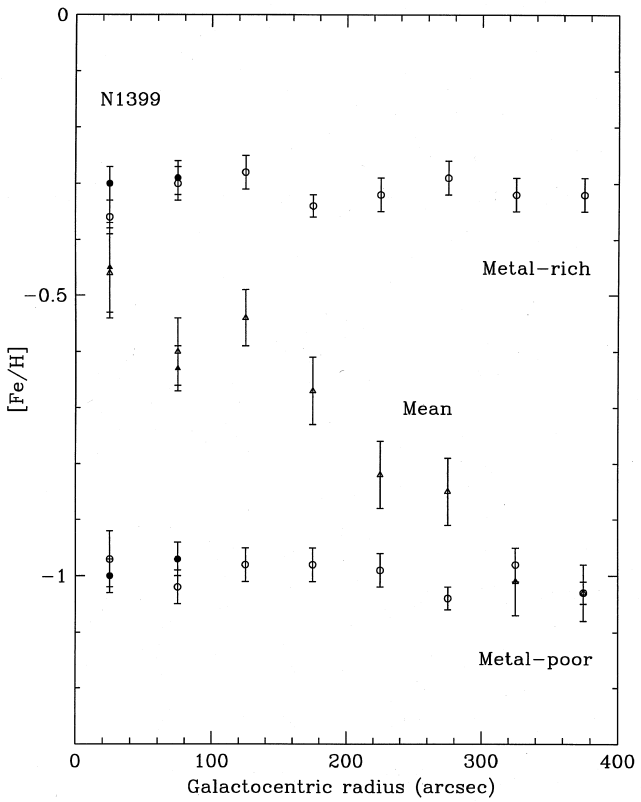

Figure 12. Radial variation of metallicity for the globular cluster subpopulations in NGC 1399. The filled circles show the *HST* data, and the open circles the CTIO data. The metal-rich, metal-poor and mean for the whole globular cluster system are shown. The mean metallicity gradient is consistent with the changing relative proportions of the subpopulations with galactocentric radius.

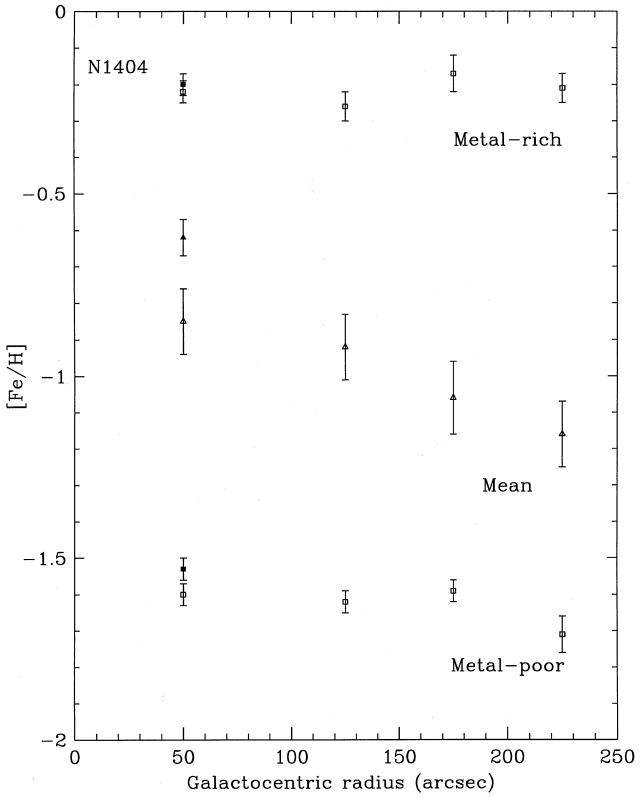

Figure 13. Radial variation of metallicity for the globular cluster subpopulations in NGC 1404. The filled circles show the *HST* data, and the open circles the CTIO data. The metal-rich, metal-poor and mean for the whole globular cluster system are shown. The mean metallicity gradient is consistent with the changing relative proportions of the subpopulations with galactocentric radius.

[Fe/H] $= +0.2 \pm 0.9$. This is similar to the metallicity derived from $B-I$ colours of the galaxy (from our CTIO data and from Goudfrooij et al. 1994). For NGC 1404, the galaxy $B-I$ colours indicate [Fe/H] ~ -0.2. Thus for both galaxies, the field stars appear to have similar metallicities to those of metal-rich GCs (which have [Fe/H] ~ -0.1).

3.3 Comparison with globular cluster formation scenarios

3.3.1 The merger model

The merger model of Ashman & Zepf (1992) and Zepf & Ashman (1993) makes some specific predictions concerning the properties of GCs in ellipticals that are the result of a gaseous merger. One of their key predictions is that ellipticals will have multimodal GC metallicity distributions. Furthermore, the metal-rich GCs will be centrally concentrated, and the more metal-poor ones will be preferentially located at large galactocentric radii. This indeed appears to be the case for both NGC 1399 and NGC 1404, and is therefore in qualitative agreement with their model. For NGC 1404 with a low S_N value (i.e., 2.0 ± 0.5), Ashman & Zepf expect slightly fewer metal-rich (new) than metal-poor (old) GCs. Our data are generally consistent with this expectation. For NGC 1399 with $S_N = 11.5 \pm 1.0$, they would expect $N_R/N_P \sim 3$–4. In the central regions of NGC 1399 such a ratio may hold, but globally $N_R/N_P < 1$. This is, of course, complicated by the difficulty in defining clear metal-rich and metal-poor GC subpopulations. However, there seems to be a shortfall in the number of newly created GCs if gaseous mergers are responsible for the metal-rich GCs and the high S_N value. Another expectation from their merger model is that the galaxy starlight and GC system should have a similar spatial distribution in galaxies with high S_N values (i.e., those galaxies in which large numbers of new GCs should have been created by the merger). Thus we might expect the surface density of GCs to match that of the galaxy surface brightness profile for NGC 1399 but not for NGC 1404. Our data indicate that for both galaxies the GC distribution is notably flatter than the underlying starlight. We might also expect the metal-rich GCs, which should have formed from the gas of the progenitor galaxies, to reveal a radial metallicity gradient as the formation process should be dissipative. Figs 12 and 13 suggest that there is little or no metallicity gradient for the metal-rich GCs in either galaxy.

To summarize, the GC systems in NGC 1399 and NGC 1404 reveal some properties that are consistent with the Ashman & Zepf (1992) merger model, but there are also notable conflicts. On an individual basis, some of the disagreements with the model may be accommodated by

slight modifications to the initial model (see Zepf, Ashman & Geisler 1995). Forbes et al. (1997b) have recently investigated whether a sample of elliptical galaxies meets the general predictions of the Ashman & Zepf model, and the concluded that mergers were *unlikely* to account for the GC systems in large elliptical galaxies. They favoured a multiphase collapse scenario. Next, we compare the data for NGC 1399 and NGC 1404 with this scenario.

3.3.2 The multiphase collapse model

Forbes et al. (1997b) have proposed that GCs in ellipticals form *in situ* during a multiphase collapse. In the first pregalactic phase, metal-poor GCs are formed and later on, in the second galactic phase, the metal-rich GCs form. This leads to a bimodal metallicity distribution with the metal-rich GCs more centrally concentrated than the metal-poor ones. In massive ellipticals the collapse could be largely dissipationless, and so no strong radial abundance gradients are expected. The radial distribution of (the metal-poor) GCs will be more extended than the galaxy itself if, as expected, they form before the galactic stars. The overall metallicity and spatial properties of GCs derived from our data are consistent with this picture.

For cD galaxies, such as NGC 1399, Forbes et al. (1997b) suggested an additional source of GCs from tidal stripping of nearby galaxies. They suggested that some of GC subpopulation identified by Ostrov et al. (1993) at around [Fe/H] ~ -0.8 were acquired from NGC 1404 and possibly other Fornax galaxies. Recently, Jones et al. (1997) have interpreted the asymmetric X-ray emission around NGC 1404 as evidence for tidal interaction with NGC 1399. The idea of tidal stripping of GCs is given some support by our new data. The outer regions of NGC 1404 are dominated by metal-poor GCs, and it is these GCs that may be preferentially stripped and captured by NGC 1399. Thus some of the GCs in NGC 1399 with this intermediate metallicity may have originated from NGC 1404. We confirmed that NGC 1404 has a remarkably low specific frequency value ($S_N = 2.0 \pm 0.5$) for a cluster elliptical, suggesting that some GCs may have been lost. If NGC 1404 originally had $S_N = 5$, i.e., typical of normal ellipticals outside of the Fornax cluster, then it has lost $\sim$1000 GCs, which may have been tidally captured by NGC 1399. If we assume that the GC system and galaxy starlight originally (i.e. before tidal stripping) continued beyond 4 arcmin with the same slope as found in Section 3.1, then we can calculate the S_N value of the stripped GCs. We find that the stripped GCs are unlikely reach values of $S_N \sim 11.5$ in sufficient numbers to have an appreciable effect on the specific frequency of NGC 1399. We expected the GC surface density profile to match that of the underlying starlight in the inner regions of NGC 1404, but it appears to be somewhat flatter than the stellar profile (at least for galactocentric radii of less than $\sim$150 arcsec). This may just be indicating that tidal stripping has not yet affected the galaxy inner regions. The above circumstantial evidence suggests that NGC 1399 has acquired GCs from NGC 1404, although this is unlikely to explain the high specific frequency of NGC 1399. Large samples of GC metallicity and kinematic information from spectra are probably required before the multiphase collapse and tidal stripping ideas can be fully tested.

4 CONCLUSIONS

We present new optical data of the globular cluster (GC) systems in NGC 1399 and NGC 1404. Our images were taken in *B* and *I* filters using the *Hubble Space Telescope* (*HST*) and the 1.5-m telescope at Cerro Tololo Inter-American Observatory (CTIO). This provides us with high spatial resolution in the central regions and wide-area coverage respectively. From the *HST* data we have detected over 500 GCs in NGC 1399, and over 200 in NGC 1404, covering $\sim$90 per cent of the GC luminosity function. With the aid of an *HST* background field of the same exposure time, we estimate that the contamination levels in the *HST* samples are only a few per cent.

Both galaxies reveal a broad GC colour/metallicity distribution. These distributions are *inconsistent* with a single Gaussian. For NGC 1399, two Gaussians with mean metallicities of [Fe/H] ~ -1.1 and -0.1 provide a reasonable representation of the data, although a multimodal distribution with several different GC subpopulations remains a possibility. In the case of NGC 1404 we tentatively claim evidence for a bimodal GC distribution with the metal-poor population around [Fe/H] ~ -1.5 and the metal-rich population at [Fe/H] ~ -0.1. In both galaxies the different metallicity peaks are consistent with distinct GC subpopulations in which the metal-rich GCs are more centrally concentrated than the metal-poor ones. Globally, the GC systems reveal metallicity gradients. However, these gradients are consistent with a changing relative mix of the two GC subpopulations with galactocentric radius.

We derive GC surface density profiles, and show them to be flatter (i.e., more extended) than the underlying starlight. The total number of GCs and specific frequency are calculated to be $N = 5700 \pm 500$, $S_N = 11.5 \pm 1.0$ for NGC 1399, and $N = 725 \pm 145$, $S_N = 2.0 \pm 0.5$ for NGC 1404. Finally, we discuss our results in the context of two GC formation scenarios. The GC data on NGC 1399 and NGC 1404 are generally more consistent with a multiphase collapse (e.g. Forbes et al. 1997b) than a merger (e.g. Ashman & Zepf 1992) origin.

ACKNOWLEDGMENTS

We thank M. Kissler-Patig and M. Rabban for help and useful discussions. We also thank the referee, T. Bridges, for several helpful comments. This research was funded by the *HST* grant GO-05990.01-94A.

REFERENCES

Ashman K. M., Zepf S. E., 1992, ApJ, 384, 50
Ashman K. M., Bird C. M., Zepf S. E., 1994, AJ, 108, 2348
Brodie J. P., Huchra J., 1991, ApJ, 379, 157
Bridges T. J., Hanes D. A., Harris W. E., 1991, AJ, 101, 469
Couture J., Harris W. E., Allwright J. W. B., 1990, ApJS, 73, 671
de Vaucouleurs A., Longo G., 1988, Catalogue of Visual and Infrared Photometry of Galaxies from 0.5 μm to 10 μm. University of Texas, Austin
Elson R. A. W., Santiago B. X., 1996, MNRAS, 280, 971
Elson R. A. W., Grillmair C. J., Forbes D. A., Rabban M., Williger G. M., Brodie J. P., 1997, MNRAS, in press
Faber S. M. et al., 1989, ApJS, 69, 763
Forbes D. A., Franx M., Illingworth G. D., 1995, AJ, 109, 1988

Forbes D. A., Brodie J. P., Huchra J., 1996a, AJ, 112, 2448
Forbes D. A., Brodie J. P., Grillmair C. J., 1997b, AJ, 113, 1652
Forbes D. A., Brodie J. P., Huchra J., 1997a, AJ, 113, 887
Forbes D. A., Franx M., Illingworth G. D., Carollo C. M., 1996b, ApJ, 467, 126
Forte J. C., Martinez R. E., Muzzio J. C., 1982, AJ, 87, 1465
Geisler D., Forte J. C., 1990, ApJ, 350, L5
Geisler D., Lee M. G., Kim E., 1996, AJ, 111, 1529
Goudfrooij P., Hansen L., Jorgensen H. E., Norgaard Nielson H. U., de Jong T., van den Hoek L. B., 1994, A&AS, 104, 179
Grillmair C., Pritchet C., van den Bergh S., 1986, AJ, 91, 1328
Grillmair C. et al., 1994a, ApJ, 422, L9
Grillmair C. et al., 1994b, AJ, 108, 102
Grillmair C., Forbes D. A., Brodie J. P., Elson R. A. W., 1997, AJ, submitted
Hanes D. A., Harris W. E., 1986, ApJ, 309, 564
Harris W. E., van den Bergh S., 1981, AJ, 86, 1627
Huchra J., Brodie J. P., Kent S., 1991, ApJ, 370, 495
Ikebe Y. et al., 1996, Nat, 379, 427
Jacoby G. H. et al., 1992, PASP, 104, 599
Jones C., Stern C., Forman W., Breen J., David L., Tucker W., Franx M., 1997, ApJ, 482, 143
Kissler-Patig M. et al., 1997, A&A, 319, 470
Lilly S. J., Le Fèvre O., Crampton D., Hammer F., Tresse L., 1995, ApJ, 455, 50
Longo G., de Vaucouleurs A., 1983, A General Catalogue of Photometric Magnitudes and Colours in the *UBV* System. University of Texas, Austin
Mason K. O., Rosen S. R., 1985, Space Sci. Rev., 40, 675
Ostrov P., Geisler D., Forte J. C., 1993, AJ, 105, 1762
Richtler T., Gerbel E. K., Domgorgen H., Hilker M., Kissler M., 1992, A&A, 264, 25
Wagner S., Richtler T., Hopp U., 1991, A&A, 241, 399
West M. J., Cote P., Jones C., Forman W., Marzke R. O., 1995, ApJ, 453, L77
Whitmore B. C., Sparks W. B., Lucas R. A., Macchetto F. D., Biretta J. A., 1995, ApJ, 454, L73
Zepf S. E., Ashman K. M., 1993, MNRAS, 264, 611
Zepf S. E., Ashman K. M., Geisler D., 1995, ApJ, 443, 570